I&EC research
Industrial & Engineering Chemistry Research
pubs.acs.org/IECR
Article

Improvement of Ni/Al_2O_3 Catalysts for Low-Temperature CO_2 Methanation by Vanadium and Calcium Oxide Addition

Gabriella Garbarino, Paweł Kowalik, Paola Riani, Katarzyna Antoniak-Jurak, Piotr Pieta, Agnieszka Lewalska-Graczyk, Wojciech Lisowski, Robert Nowakowski, Guido Busca,* and Izabela S. Pieta*

Cite This: *Ind. Eng. Chem. Res.* 2021, 60, 6554−6564

Read Online

ACCESS | Metrics & More | Article Recommendations | Supporting Information

ABSTRACT: CO_2 methanation is a very promising technology for the production of alternative fuels with the simultaneous use of greenhouse gases. Therefore, intensive research is carried out on the optimization of catalysts with excellent properties for operation in the area of low temperatures. Here, we present research on a catalyst composed of 19 wt % NiO supported on alumina/calcium aluminate. The catalyst was modified with V_2O_5 in order to be suited for extrusion and scale-up in the frame of power to gas technology. Samples with various vanadium contents (Ni−*x*V, where *x* represents the amount of vanadium) were prepared in the form of ground granules obtained from 0.5 mm diameter spherical grains. X-ray diffraction (XRD), transmission electron microscopy (TEM), skeletal infrared (IR), diffuse reflectance ultraviolet−visible-near-infrared (DR-UV−vis-NIR), and X-ray photoelectron (XPS) spectroscopies, as well as H_2 temperature-programmed reduction (H_2-TPR), were used to characterize the samples. Catalytic performances of the catalyst samples were tested in CO_2 hydrogenation at 1 atm. Among the many supported Ni catalysts tested in our laboratories, the catalysts of 0.5 and 1 wt % V showed very high activity, with the highest CH_4 yield of 97% at 623 K. These catalysts exhibited 100% CH_4 selectivity up to 673 K. The excellent performances of the studied catalysts are attributed to the possible formation of Ni−V solid solution alloy nanoparticles.

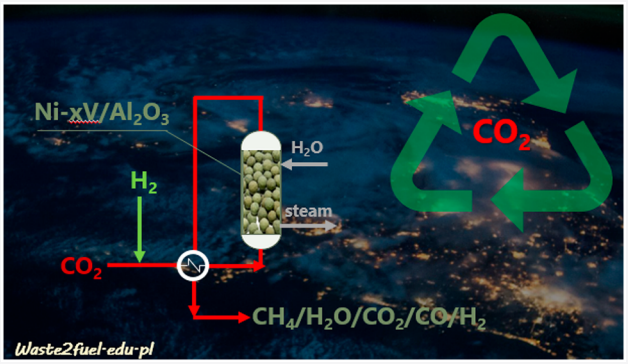

INTRODUCTION

CO_2 and CO methanation over nickel as a catalyst was first described by Sabatier and Senderens.[1,2] Since the mid-1960s, carbon oxides (CO_x) methanation has been used in the preparation of N_2 + H_2 ammonia synthesis gas to remove residual carbon oxides, usually at a very low concentration (<0.5% vol).[3] All producers of industrial catalysts commercialize various types of Ni-based methanation catalysts of different Ni contents.[4−6] The 25 wt % NiO on alumina spheres (METH 134) is offered for activity above 473 K and a 43% NiO/Al_2O_3 catalyst (METH135) for enhanced activity at low temperatures suitable for higher space velocities. The 0.3% Ru on alumina tablets (METH150) presents high activity at extremely low temperatures (below 443 K).[4] Methanation can also be realized under similar conditions for CO_x removal from hydrogen produced during the steam cracking processes[5] and from hydrogen dedicated for fueling PEM fuel cells.[7] The RANG and RANG-PR series catalysts are designed for deep removal of CO_x from hydrogen and synthesis gases by conversion to methane.[6] This process, as the final stage of the purification of process gases from CO_x, is of extreme importance in ammonia plants, enhancing the ammonia synthesis process efficiency.[6] Exothermic CO_x methanation, coupled with previous endothermic methane steam reforming, was considered as a pathway to transport and regenerate nuclear energy from nuclear fission power stations to cities in the so-called ADAM-EVE project.[8]

The conversion of syngases (concentrated $CO/CO_2/H_2$ mixtures) from coal gasification to synthetic methane (or substitute natural gas, SNG) was developed during the oil crises of the 1970s. A commercial synthetic gas plant was opened in 1984 and is still operating in Beulah, North Dakota, USA.[9] Several companies developed SNG technologies, also known as "high-temperature methanation", i.e., Johnson Matthey's DAVY[10] or Topsoe's TREMP.[11] Also, several plants are under construction or are already operating in China to produce SNG from coal.[9] The SNG production from biomass gasification syngases was also realized, at least at the pilot plant level.[9,12] In

Special Issue: Enrico Tronconi Festschrift

Received: November 11, 2020
Revised: April 2, 2021
Accepted: April 5, 2021
Published: April 16, 2021

https://doi.org/10.1021/acs.iecr.0c05556
Ind. Eng. Chem. Res. 2021, 60, 6554−6564

recent years, the methanation of CO_2 from combustion plants using hydrogen produced by water electrolysis, powered by photovoltaic or eolic energy (power to gas), has been of great interest.[13−15] This approach is considered as carbon dioxide reuse catalytic technology that enables greenhouse gas emissions reduction and ensures more efficient energy transport. This is one of the many applications of heterogeneous catalysis that can be applied in the near future for sustainable and environmentally friendly energy production and management. Enrico Tronconi and his co-workers have made a very important contribution in this broad field in the last 40 years.

The CO_2 methanation reaction is also considered by NASA to regenerate water in spacecrafts using CO_2 from astronauts' respiration and hydrogen from the oxygen generation system by water electrolysis.[16] It can also be applied to convert biogas to biomethane.[17] In our previous studies, we characterized Ni/γ−Al_2O_3 catalysts and their activity in CO_2 methanation under atmospheric pressure,[18] also in comparison with Ru/γ-Al_2O_3 catalysts.[19] Moreover, we reported efforts to improve Ni/γ−Al_2O_3 catalysts' activity and selectivity by adding silica and lanthana to catalyst formulation.[20,21] Calcium aluminates are reported to represent useful stabilizing supports for commercial extruded Ni-based catalysts to be used in steam reforming reactions (SR).[22−27] Moreover, such stabilization has been proven in a pilot-test study applying both laboratory and industrial testing protocols.[23−27] We found that catalysts, which are primarily designed for both methane or biogas reforming, are also active in CO_2 methanation.[6,23−27] In this article, we report on the addition of vanadium oxide (V_2O_5) on the Ni/CaO−Al_2O_3 system in order to optimize the catalyst for CO_2 methanation and improve its selectivity toward methane. We placed particular attention on the reaction study in the low-temperature region where the reaction is kinetically limited. Similar catalysts were previously tested, exhibiting promising performance for both hydrogenation and reforming reactions.[24−27]

MATERIALS AND METHODS

The catalysts were designed, synthesized, and characterized both in powder and structured form by Waste2Fuel and Ł-INS Pulawy laboratories as reported previously.[6,24−27] The vanadium (V) and calcium (Ca) oxide-containing NiO/Al_2O_3 catalysts series were prepared by a multistep combined technique.[27] Considering that the Ca content is the same for all samples, the samples are denoted as Ni−xV, where x represents the nominal V content in the catalyst (0, 0.5, 1, and 3 wt %). In the first stage, a Ni−Al hydroxycarbonate precursor was synthesized by coprecipitation from an aqueous nickel nitrate solution with a sodium aluminate and sodium carbonate solution in a controlled pH range of 8.0−8.5 and at a temperature of 348 ± 5 K. The obtained precipitate was washed with distilled water to achieve filtrate conductivity below 300 μS/cm. The precursor slurry was subjected to spray calcinations at 723 K, and a fine-grained Ni−Al mixed oxide powder (d_{50} = 40 μm) was obtained. Then, three powders of Ni−Al oxide, Pural SB boehmite alumina (d_{50} = 45 μm), and monocalcium aluminate $CaAl_2O_4$ (d_{50} = 45 μm) in the weight ratio of 1.33/3.33/1.00 were homogeneously mixed during 8 h (Zet mixer). The obtained mixture was formed into spherical grains by wetting with redistilled water as granulation fluid using a Erveka AR 403 pan granulator. The spherical precatalyst was dried at 378 K for 24 h, and then, a fraction of 5.0 ± 0.5 mm in diameter was separated and subsequently treated.

Such an obtained precatalyst was divided into three parts. Each part was introduced into a different aqueous solution of ammonium metavanadate (99% purity, Standard, Lublin, Poland) and oxalic acid (99% purity, POCH, Gliwice, Poland) with a constant molar ratio of $NH_4VO_3/C_2H_2O_4{\cdot}2H_2O$ = 0.5 and heated to a temperature in the range of 328 ± 5 K. The single incipient wetness impregnation was sufficient to prepare the catalysts of nominal V content of 0.5 and 1 wt %, but in order to prepare the catalyst of higher vanadium loading (3 wt %), double impregnation was performed. After each impregnation, the Ni−V−Al samples were dried at 393 K for 12 h and subsequently calcined at 773 K for 3 h.

Characterization. X-ray diffraction (XRD) patterns were collected using a D5000 powder diffractometer (Bruker AXS) equipped with a LynxEye strip detector. Cu Kα radiation was used with an X-ray tube operating at 40 kV and 40 mA. XRD patterns of the spent catalysts were collected by means of an X'Pert vertical powder diffractometer. Diffractograms were collected in the 15−100° 2θ range with a step size of 0.03° and a counting time for each step of at least 19 s. Measurements were always performed in the Bragg−Brentano geometry. Powder patterns were indexed by comparing experimental results to the data reported in the JCPDS or in the Pearson's Crystal Data database.

Microscopic images of fresh catalysts were obtained using a HRTEM TITAN 60−300 instrument with a X-FEG-type emission gun operating at 80 kV. This microscope is equipped with a Cs image corrector and a STEM high-angle annular dark-field detector (HAADF); its point resolution is 0.06 nm in TEM mode. For HRTEM analysis, the powder samples were dispersed in ethanol and sonicated for 5 min. One drop of the resulting solution was then placed on a copper grid with a holey carbon film, after which the sample was dried at room temperature.

Morphology and composition of the spent catalyst were investigated by a Zeiss SUPRA 40 VP scanning electron microscope, equipped with a field emission gun, a high sensitivity "InLens" secondary electron detector, and an OXFORD "INCA Energie 450 × 3" spectrometer. Samples powders were directly mounted on high purity conductive double-sided adhesive carbon tabs and then analyzed.

XPS measurements were performed to determine the chemical state of the elements in the studied samples by a Microlab 350 instrument (Thermo Electron). XPS spectra were acquired using Al Kα ($h\nu$ = 1486.6 eV) radiation. Survey spectra and high-resolution spectra were recorded using pass energies of 100 and 40 eV, and the XPS signal intensity was determined using linear or Shirley background subtraction. Peaks were fitted using an asymmetric Gaussian/Lorentzian mixed function, and the measured binding energies were corrected based on the C 1s energy at 285.0 eV.

FT-IR spectra were registered with a Nexus Thermo Fisher instrument with 100 scans and spectra resolution of 2 cm^{-1}. KBr pressed disks were used for skeletal characterization.

DR-UV−vis-NIR spectra were collected with a JASCO V570 instrument equipped with an integrating sphere. The samples were gently pressed into the sample holder.

Hydrogen temperature-programmed reductions (H_2-TPR, in 5% H_2 in He) were performed in a quartz tube reactor connected to a quadrupole mass spectrometer (HPR 60, Hiden). Here, 45 mg of the catalyst sample was used for each test. These samples were heated from RT to 773 K with a ramp rate of 10 K min^{-1}.

https://doi.org/10.1021/acs.iecr.0c05556
Ind. Eng. Chem. Res. 2021, 60, 6554−6564

Catalytic Tests. Catalytic tests reported here have been realized in a Genoa laboratory, while chemisorption and specific activity data for the Ni−*x*V catalysts were conducted by Waste2Fuel and Ł-INS Pulawy laboratories as reported previously.[6,17−20,25−27] A tubular silica glass flow reactor containing a fixed bed with 88.2 mg of catalyst mixed with 700 mg of silica glass beads of 0.25−0.21 mm (Sigma-Aldrich, calcined 1073 K for 5 h) was used in steady-state catalytic experiments. Prior to catalytic experiments, catalysts were reduced in a H_2/N_2 atmosphere (1023 K for 30 min). CO_2 hydrogenation experiments were conducted with the following feeds: 6% CO_2, 30% H_2, and N_2 balance used as a carrier gas. The gas hourly space velocity (GHSV) was equal to 55,000 h^{-1} (273 K and 1 atm, catalyst volume 0.85 cm^3). In order to follow any hysteresis, activation, or short-term deactivation effects, experiments were performed both in ascending and descending reaction temperatures (523, 573, 623, 673, 723, 773 K and reverse). The full experiment indicates 7 h time on stream. The online products analyses were performed using a Nicolet 6700 FT-IR instrument. The frequencies at which CO_2, CH_4, and CO molecules absorb weakly were used: 2293, 2170, and 1333 cm^{-1} for CO_2, CO, and CH_4, respectively, after subtraction of the baseline, with previous calibrations using gas mixtures with known concentrations in order to have quantitative results. Produced water was condensed upstream of the IR cell.

RESULTS AND DISCUSSION

The XRD patterns of the Ni-precatalyst and full composition Ni−*x*V catalysts are shown in Figure 1. The data showed characteristic signals of calcite ($CaCO_3$, JCPDS 98-002-0179) and NiO (JCPDS 98-024-6910) at 29.3°, 39.6°, 47.2°, 48.1°, 58.5°, 60.1°, 64.2°, and 37.3°, 63.2°.[27,28]

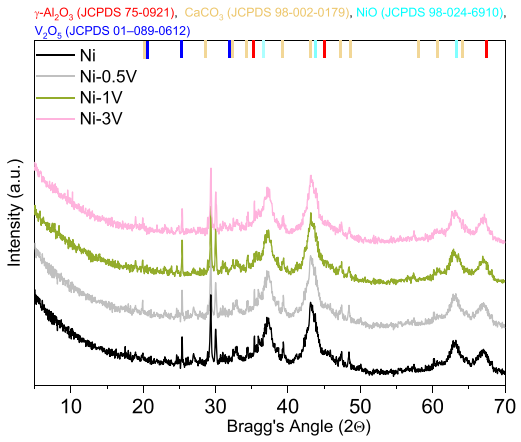

Figure 1. XRD patterns of the fresh Ni−*x*V catalysts. JCPDS reference diffraction patterns are included for comparison purposes.

The diffraction peaks at 37.5°, 39,7°, 46.7°, and 66.3° (2θ) of the alumina oxide phase corresponding to γ-Al_2O_3 (JCPDS 75-0921)[28] are mostly overlapped by calcite. Peaks related to vanadium species at 21.3°, 26.7°, and 36.2° (2θ) assigned to the V_2O_5 phase (JCPDS 01-089-0612) were detected with very weak intensities. The peak at around 30° can be attributed to the presence of $CaAl_2O_4$ (JCPDS 53-0191).[27] Moreover, the two peaks at (2θ), 20° and 26°, well distinguishable in all the diffraction patterns, can be assigned to the presence of Ca_2AlO_7 (Ca_2AlO_7, mS48).

The skeletal infrared (IR) spectra of the samples are reported in Figure 2. The vanadium-containing samples show the bands of calcite (1460, 1410, 874, 724 cm^{-1}),[29] alumina (broad feature around 800 cm^{-1} with a strong absorption down to 500 cm^{-1}),[30] and NiO (strong absorption at 500−400 cm^{-1}),[31] in line with the XRD analysis. Also, the spectrum of the V-free sample shows the features of the $Al(OH)_3$ hydroxide gibbsite (1026 cm^{-1}), AlO(OH) oxy-hydroxide boehmite (1072, 744 cm^{-1}),[32] and carbonate species (1500−1400 cm^{-1}) together with Al−O stretching modes (600−500 cm^{-1}). It seems likely that this solid underwent rehydration after the preparation procedure.

DR-UV−vis-NIR spectra of the investigated catalysts are reported in Figure 3. In the UV range (240−300 nm), the V-containing samples show a strong absorption at ∼280 nm. This band is associated with two superimposed charge transfer transitions (CT), i.e., O^{2-} (2p) → Ni^{2+}(3d)[31] and O^{2-} (2p) → V^{5+}(3d).[33] The presence of dispersed vanadyl centers was superimposed, as confirmed by the slight increase of the band ∼280 nm upon increasing vanadium content. The Ni-3 V sample shows an additional tail extended up to 560 nm, likely due to condensed V_xO_y species.[33] In the visible range, these samples show absorptions in the region of the d → d transitions of Ni^{2+}. In particular, the two features at 650 and 722 nm correspond well to those reported for bulk NiO.[31] At the same time, no evidence of Ni^{2+} in the defective aluminate structure, usually predominant in NiO/Al_2O_3 systems, was found. This is in agreement with the adopted synthesis procedure.

A different spectrum is observed for the vanadium-free sample (Ni precatalyst). While the absorption in the UV range is far weaker, the absorption in the visible range is strong, continuous, and featureless, in agreement with the sample's almost black color. We found a similar spectrum in the case of other, mostly amorphous samples, i.e., in the Ni−La/Al_2O_3 system, attributed to nickel-containing defective perovskite-type structures.[34] The IR and UV−vis-NIR results are consistent, suggesting that the structural and electronic composition of the V-free sample is different from that of the V-containing samples. However, this difference is not evident in the XRD patterns, suggesting the possible presence of the amorphous phases.

Figure 4 shows TEM images collected for the fresh Ni and Ni−*x*V catalysts. For all Ni−*x*V catalysts, the morphology of the support was similar, and mostly calcite appeared as particles with the largest thickness. The Ni and/or V components were detected as homogeneously distributed dark particles with spherical structures. The measured NiO particle size was in the range of 7−11 nm in diameter ($D_{P\text{-}NiO}$), as reported in Table 1.

The EDX analysis performed during the TEM study (Figure 5) revealed the presence of vanadium and nickel only for the sample with the highest vanadium content, i.e., Ni-3 V. The lack of V and Ni signals for Ni−*x*V samples with a lower V content is due to the small amount of the vanadium oxide precursor used in the catalyst preparation compared to the amount of Ni and Al.[27] The features at 1 and 8 keV are assigned to copper, used as a sample holder for the TEM analysis. The differences in the EDX spectra collected on the single particle (curves 2 in Figure 5) and the sample bulk (curves 1 in Figure 5) indicate the sample heterogeneity resulting from the adopted synthesis for a pelletized catalysts.[27]

The Ni 2p core-level XPS spectra, due to the Ni 2p3/2 and Ni 2p1/2 doublet and their shakeup satellites, are reported in Figure 6. The splitting of the peak at 854−856 eV indicates that two different types of Ni species can be distinguished for all investigated catalyst samples. One, with signals at 854.6−855.4

https://doi.org/10.1021/acs.iecr.0c05556
Ind. Eng. Chem. Res. 2021, 60, 6554−6564

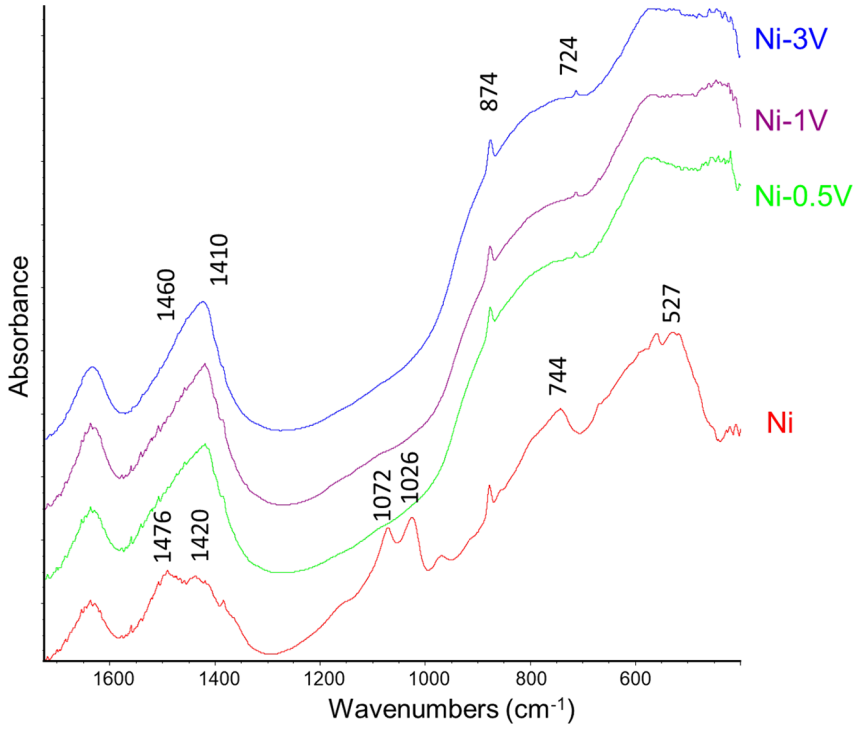

Figure 2. Skeletal IR spectra of Ni−*x*V catalysts in the range of 1700−400 cm^{-1}.

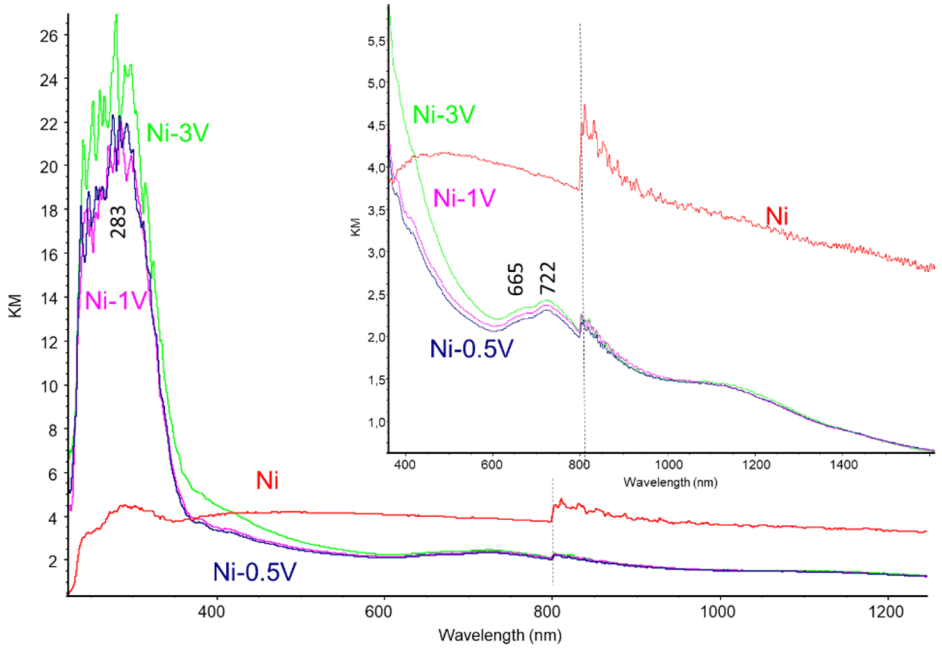

Figure 3. DR-UV−vis-NIR spectra of fresh Ni−*x*V catalysts. In the inset, vis-NIR regions are magnified.

eV, is related to Ni^{2+} (NiO) and, the second, at 856.1−856.4 eV, is associated with Ni^{2+}, which strongly interacts with alumina or in the form of the spinel $NiAl_2O_4$, whose formation is limited to a near-surface layer as discussed previously.[24,28,35] For the investigated catalysts, the most intense peak is associated with Ni^{2+} as NiO, revealing that NiO species are present on the catalysts surfaces in a higher proportion compared to spinel-type species. The Ni^{2+} oxidic-to-spinel ratio increases with the increase of the vanadium content (Figure S1). This could be indicative that the vanadium incorporation prevents the formation of hardly reducible spinel.[24]

Figure 7 shows deconvoluted high-resolution XPS spectra of the O 1s and V 2p binding energy for the Ni-3 V catalyst. For all Ni−*x*V samples, vanadium was detected as $V^{3+}(V_2O_3)$, $V^{4+}(VO_2)$, and $V^{5+}(V_2O_5)$ with a peak located at 515.6−515.7, 516.2−516.4, and 516.9−517.2 eV, respectively. Moreover, the population of each species was similar for all catalysts, regardless of the vanadium content. However, the presence of vanadium influences the binding energy (BE) and shape of the O 1s peak. It can be noticed that for a higher vanadium content, the O 1s peak is red-shifted ca. 4 eV. Moreover, the peak at 530 eV becomes more pronounced following the order Ni-3 V > Ni-

https://doi.org/10.1021/acs.iecr.0c05556
Ind. Eng. Chem. Res. 2021, 60, 6554−6564

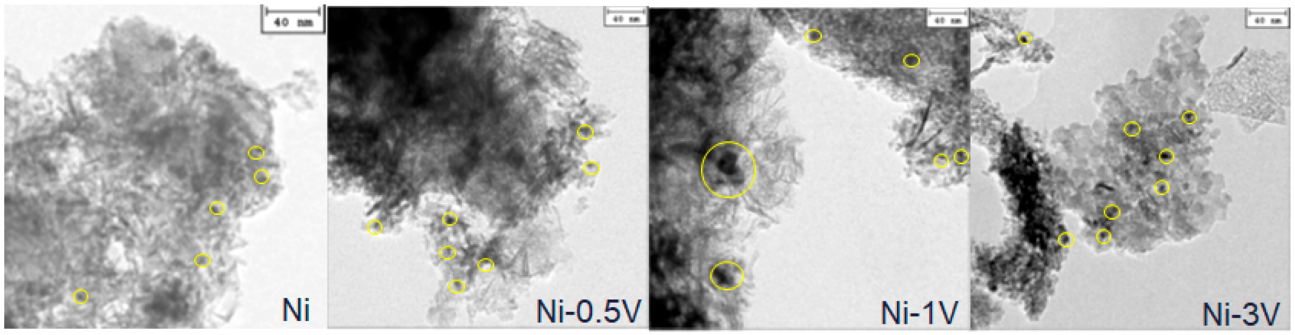

Figure 4. TEM images of fresh Ni−*x*V catalysts. Ni and/or V nanoparticles are highlighted by yellow circles.

Table 1. Physicochemical Properties of Studied Ni−*x*V Catalysts

Catalyst	Denoted	$D_{P\text{-}NiO}$, nm TEM[a]	$D_{P\text{-}NiO}$, nm XRD[b]	BET, $m^2\ g^{-1}$
Ni/Al_2O_3	Ni	<7	<8	198
Ni-0.5 V/Al_2O_3	Ni-0.5V	<11	<10	135
Ni-1 V/Al_2O_3	Ni-1V	<9	<10	135
Ni-3 V/Al_2O_3	Ni-3V	<10	<9	135

[a]Obtained from TEM. [b]Calculated from XRD diffractograms.

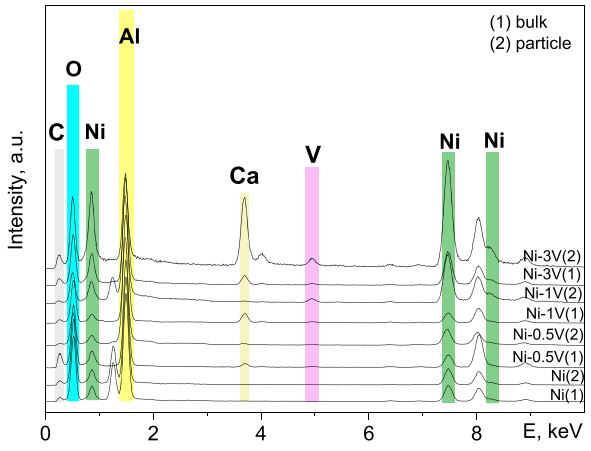

Figure 5. EDX analysis of fresh Ni−*x*V catalysts (1) on bulk and (2) on a single particle.

1 V > Ni-0.5 V > Ni. This can be directly related to the increased amount of oxidic species on the catalysts surfaces and the oxidative storage capacity of the V-modified samples.[24,27]

The reduction characteristics of the Ni−*x*V (*x* = 0, 0.5, 1, and 3) catalysts were studied over a temperature range from 298 to 773 K with a ramp rate of 10 K min^{-1}. In Figure 8, the H_2 responses as a function of temperature are presented. The TPR profiles revealed significant differences between the samples. The results show a systematic change in the reduction of Ni species with an increase in vanadium loading. Importantly, the TPR profiles, reduction temperature, and amount of hydrogen consumed were strongly influenced by the catalyst composition. The TPR profile of the reference Ni precatalyst (Figure 8) shows peaks with maxima at 583, 700, and 753 K, which can be associated with the reduction of NiO bulk, small NiO crystallites (583 K) and noncrystalline NiO (700 K) species, respectively.[36,37] The Ni^{2+} species reduction strongly interacting with alumina or $NiAl_2O_4$ reduction was evidenced far above 753 K.[26] According to the literature, the reduction of the bulk NiO is usually evidenced by the peak at ∼650 K, while the feature at ∼750 K is related to the reduction of noncrystalline NiO.[36,37] On the other hand, nickel aluminate spinel-type species are characterized by high reduction temperatures above 973 K.[38,39] In contrast, free NiO weakly interacting with the support is easily reduced at 573−623 K. Nickel species which are not completely associated with spinel are reducible at intermediate temperatures of 623−773 K. The reduction temperature differs slightly from those reported in the literature, which can be mostly related to the metal−support interaction due to the presence of Ca and modifiers.

For the Ni-0.5 V and Ni-1 V catalysts, the hydrogen consumption starts at 553 K, while for the Ni-3 V sample it is shifted toward a higher temperature by 70 K. For both Ni-0.5 V and Ni-1 V catalysts, a broad peak is observed, with maxima located at 663 K, while for Ni-3 V it is above 773 K. They can be related to NiO probably modified by V_2O_5 or to Ni−V mixed oxides.[27] Moreover, the amount of hydrogen consumed at intermediate temperatures of 600−700 K increased significantly for the Ni-0.5 V and Ni-1 V catalysts compared to that for the V-free catalyst. It suggests enhanced reducibility of the modified catalyst or an increase in the population of nickel species that are not entirely associated with aluminate spinel but associated with Ni−V mixed oxides.[40] Although V modification did not strongly influence the Ni particle size and morphology according to XPS, the vanadium presence changes both the type and population of surface Ni species (Figure S1). Presumably, V limits the Ni diffusion into the support and the hardly reducible spinel structures formation, thus producing Ni−V mixed oxides which are more easily reducible than Ni aluminate species but less than pure NiO.[27] On the other hand, it is also expected that together with Ni species V_2O_5 undergoes simultaneous reduction, which increases the H_2 uptake. For the V_2O_5/Al_2O_3 catalyst, the reduction onset was reported to occur at 600 K, and the peak maximum was located at 800 K, indicating V^{5+} to V^{3+} reduction.[41]

CO_2 Hydrogenation. The results of the online analyses by FT-IR spectroscopy of the effluent gases are presented in Figure 9. Catalytic experiments were performed on all samples with a previous step of catalyst reduction to bring Ni to its reduced state. The data are reported as absorbances of the diagnostic bands of CO_2, CH_4, and CO. The decrease in the CO_2 absorbance resulting from its conversion is accompanied by the detection of the CH_4 and CO methanation products, the absorbance of which increases correspondingly. No other C-containing products are observed in remarkable amounts (0.1 mol %). Water is a reaction product and was also quantified. Thus, the observed reactions are the methanation of CO_2 (eq 1)

https://doi.org/10.1021/acs.iecr.0c05556
Ind. Eng. Chem. Res. 2021, 60, 6554−6564

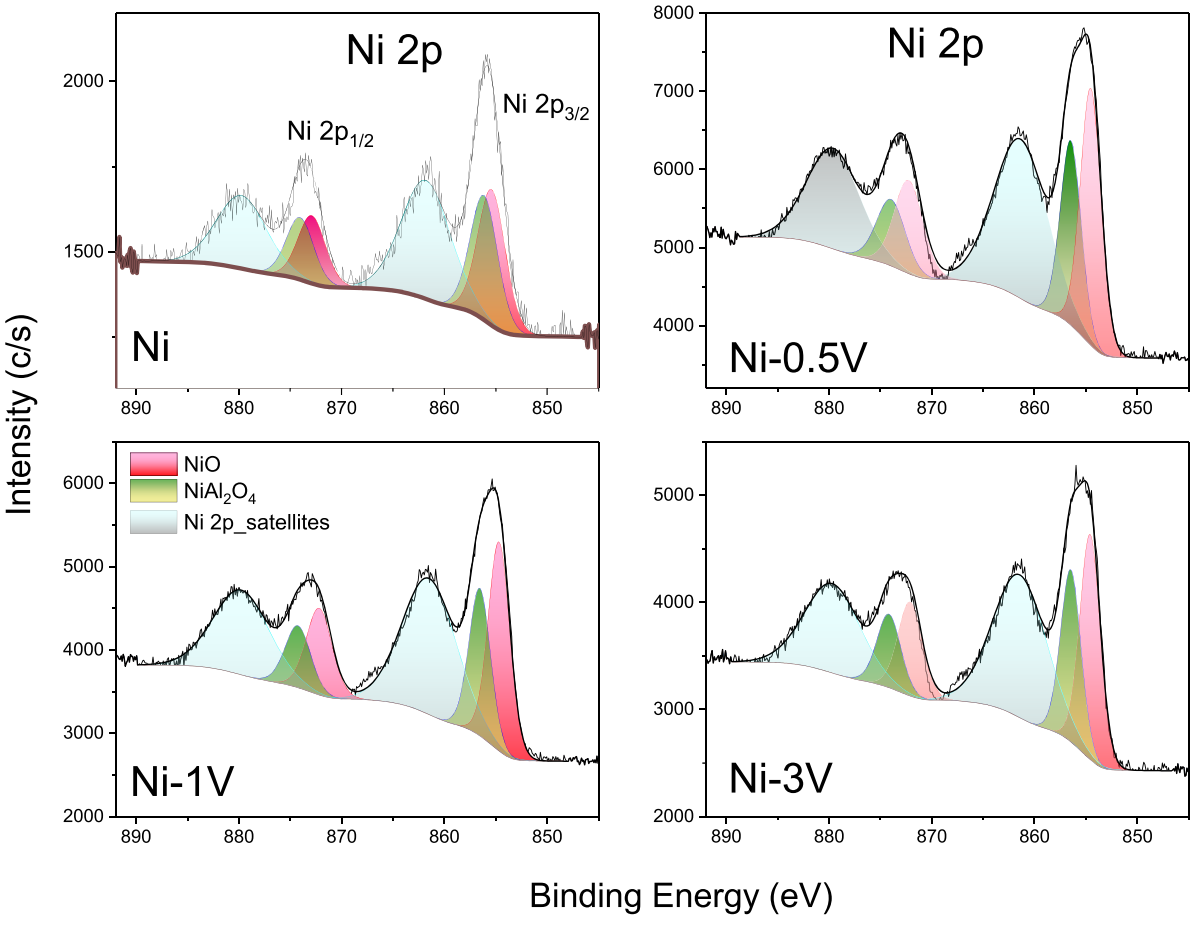

Figure 6. HR-XPS data for Ni 2p region with deconvoluted spectra for Ni and Ni−*x*V catalysts.

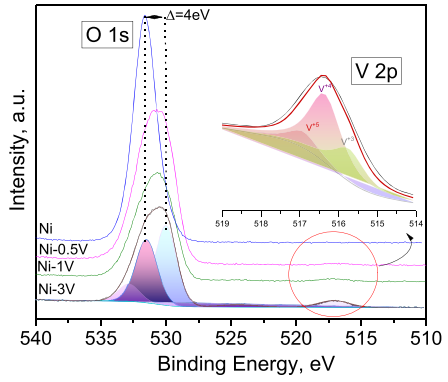

Figure 7. XPS data for O 1s and V 2p regions for fresh Ni−*x*V catalysts. The inset shows the deconvoluted V 2p spectrum for the Ni-3 V catalyst.

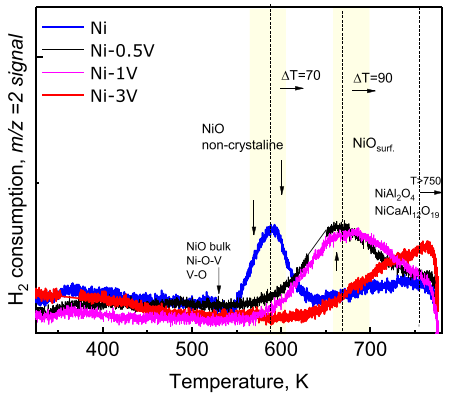

Figure 8. TPR for fresh Ni−*x*V catalysts performed for 5% H_2 + He and a flow rate of 70 mL min^{-1} at a temperature range from RT to 773 K with a ramp rate of 10 K min^{-1}. The weight of the catalyst was 45 mg.

$$CO_2 + 4H_2 \rightleftarrows CH_4 + 2H_2O \quad (1)$$

and the reverse water gas shift reaction (rWGS, eq 2)

$$CO_2 + H_2 \rightleftarrows CO + H_2O \quad (2)$$

In Table 2, the corresponding calculated values for CO_2 conversion, methane, and CO selectivities are reported. The observed data are compared with the corresponding data calculated assuming that thermodynamic equilibrium is established among CO_2, CH_4, CO, H_2, and H_2O under applied pressure, temperature, and initial composition conditions and when production of CO by rWGS is excluded.

The data show that for all catalysts at 523 and 573 K the CO_2 conversion is well lower than that allowed by thermodynamics; thus, the reaction is limited by kinetics. For these conditions, CH_4 selectivity is 100%, and CO is not observed at all. Instead, at 623 and 673 K, over Ni-0.5V and Ni-1V, the experimental data coincide, within experimental error, with those allowed by thermodynamics for the methanation reaction only, with apparently the rWGS reaction not occurring at all. When both methanation and rWGS reactions are allowed to occur, the thermodynamic equilibrium implies a small, but non-negligible, amount of CO formed. Thus, these catalysts selectively catalyze

https://doi.org/10.1021/acs.iecr.0c05556
Ind. Eng. Chem. Res. 2021, 60, 6554−6564

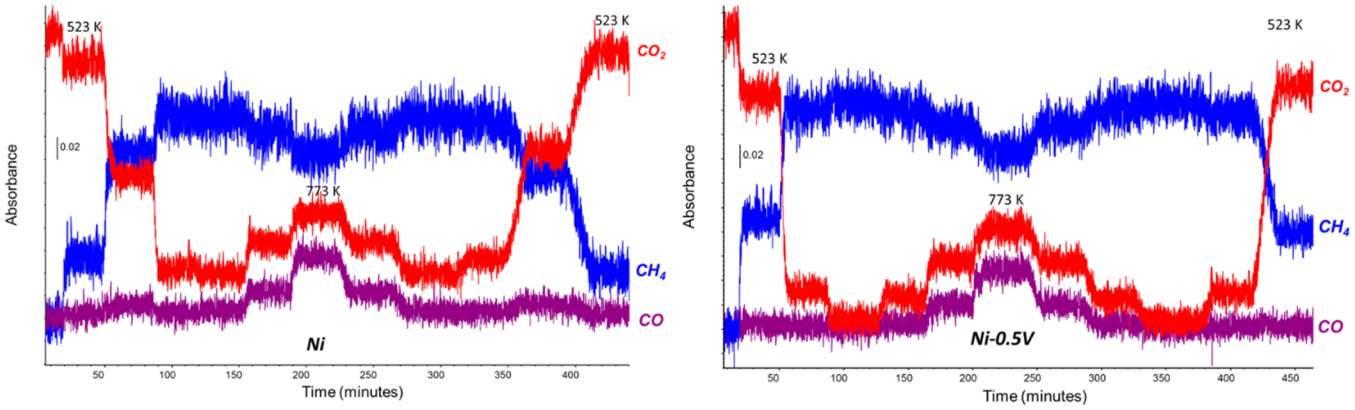

Figure 9. Online IR analyses for catalytic activities of Ni (left) and Ni-0.5 V catalysts (right). Catalyst weight was 88.2 mg. Temperature interval was 523−773 K, and GHSV was 55,000 h^{-1} (evaluated on a catalyst volume basis).

Table 2. Carbon Dioxide Conversion (X, mol %) and Selectivities (S, mol %) to Products in CO_2 Hydrogenation[a]

	Ni			Ni-0.5V			Ni-1V			Ni-3V			Thermodynamic equilibrium			Thermodynamics methanation only
T, K	X CO_2	S CH_4	S CO	X CO_2	S CH_4	S CO	X CO_2	S CH_4	S CO	X CO_2	S CH_4	S CO	X CO_2	S CH_4	S CO, %	X CO_2, %
523	12	100	0	33	100	0	31	100	0	12	100	0	99.99	100.00	0.00	99.994
573	62	100	0	91	100	0	89	100	0	67	100	0	99.80	100.00	0.00	99.8
623	87	100	0	97	100	0	97	100	0	91	100	0	97.39	99.92	0.08	97.37
673	89	100	0	93	100	0	91	100	0	90	100	0	89.89	99.20	0.80	89.58
723	80	98	2	83	99	1	82	99	1	80	98	2	79.84	95.59	4.41	78.02
773	72	89	11	74	89	11	72	89	11	71	89	11	71.27	83.60	16.40	64.81
723	81	98	2	83	99	1	81	99	1	80	98	2	79.84	95.59	4.41	78.02
673	89	100	0	93	100	0	91	100	0	89	100	0	89.89	99.20	0.80	89.58
623	84	100	0	98	100	0	98	100	0	90	100	0	97.39	99.92	0.08	97.37
573	56	100	0	91	100	0	90	100	0	59	100	0	99.80	100.00	0.00	99.8
523	7	100	0	27	100	0	24	100	0	5	100	0	99.99	100.00	0.00	99.994

[a]Experimental results and calculated data at thermodynamic equilibrium.

Table 3. Chemisorption and Specific Activity Data for Ni−*x*V catalysts[a]

	Chemisorption			Specific activity (523 K)	
Catalyst	S_{Ni}, $m^2\ g_{Ni}^{-1}$	Dispersion, %	$D_{P\text{-}Ni}$, nm	r, $\mu mol_{CO2}\ m^{-2}_{Ni}\ s^{-1}$	TOF, s^{-1}
Ni	91.1	21.3	7.4	0.357	0.0140
Ni-0.5V	75.7	19.8	8.9	1.188	0.0464
Ni-1V	72.5	15.5	9.3	1.172	0.0458
Ni-3V	63.0	12.3	10.7	0.533	0.0208

[a]S_{Ni} [m^2/g_{Ni}] is based on the assumption of complete NiO to Ni reduction before chemisorption measurements. r and TOF calculations are valid for "far from equilibrium" conditions. therefore, X_{CO2} conversions at 523 K = 0.12 were taken. r and TOF calculations were performed based on the assumptions of (a) gradientless reactor, (b) kinetic regime, and (c) $V_{inlet} = V_{outlet}$.

methanation only at temperatures up to 673 K. Moreover, although for both the V-free and Ni-3V catalysts only methane is formed, the CO_2 conversion is much lower than that allowed by thermodynamics. This suggests that an optimal vanadium content is needed to maximize methanation yield and selectivity at 623−673 K.

In the temperature range of 723−773 K, the conversion of CO_2 decreases due to thermodynamics, which becomes less favorable, and CO appears among the products. The catalysts show even slightly higher conversion than that allowed by thermodynamics, indicating a 2%−4% experimental error in the V concentration evaluation. The catalysts with intermediate vanadium content also exhibited a slightly higher conversion at these temperatures. The selectivity to CO is similar in all cases and lower than that expected by thermodynamics. A slight deactivation effect is observed for all catalysts comparing their activities at 523 and 573 K for both ascending and descending temperatures steps. However, continuous experiments showed a substantial stability of the performances for experiments during more than 30 h at 623 K.[27]

Active Ni surface area and specific activity data are collected in Table 3. The TOF value for Ni/Al_2O_3 at 513 K is equal to 0.014 s^{-1} and stays in agreement with the literature data for Ni-based catalysts varied with chemical composition and preparation method. According to Vogt et al., the TOF value at low temperature (473−573 K) for Ni deposited on different supports is in the range of 0.01−0.20 s^{-1}.[42] According to Liu et al., TOF at 503 K for 5%Ni deposited on an Al−Ca nanocomposite is equal to 1.02×10^{-3} s^{-1}.[43] Other authors provided similar values of TOF at low temperature CO_2 methanation: 0.06 s^{-1} at 548 K for 12%Ni deposited on γ-Al_2O_3,[44] 0.6−2.4 $\times 10^{-3}$ s^{-1} at 493 K for Ni/Al_2O_3 systems[45],

https://doi.org/10.1021/acs.iecr.0c05556
Ind. Eng. Chem. Res. 2021, 60, 6554−6564

Table 4. Comparison of Performances of Ni Catalysts in CO_2 Hydrogenation at 623 K and Atmospheric Pressure

Symbol	wt % Ni	Other catalysts components	Y_{CH4}, %	Y_{CO}, %	ref
Ni	19	CaO, Al_2O_3	87	0	26, this work
Ni-0.5V	15	V_2O_5 ,CaO, Al_2O_3	97	0	26, this work
Ni-1V	15	V_2O_5, CaO, Al_2O_3	97	0	26, this work
Ni-3V	15	V_2O_5, CaO, Al_2O_3	91	0	26, this work
Ni0LA	13.5	Al_2O_3	73	1	32
Ni37LSA	13.5	La_2O_3, SiO_2, Al_2O_3	90	0	20
Ni14LA	13.5	La_2O_3 ,Al_2O_3	92	0	32
JM57-4Q[a]	24	CaO, Al_2O_3	74	1	22

[a]Commercial methane steam reforming catalyst from Johnson Matthey. Ref. 22, 23.

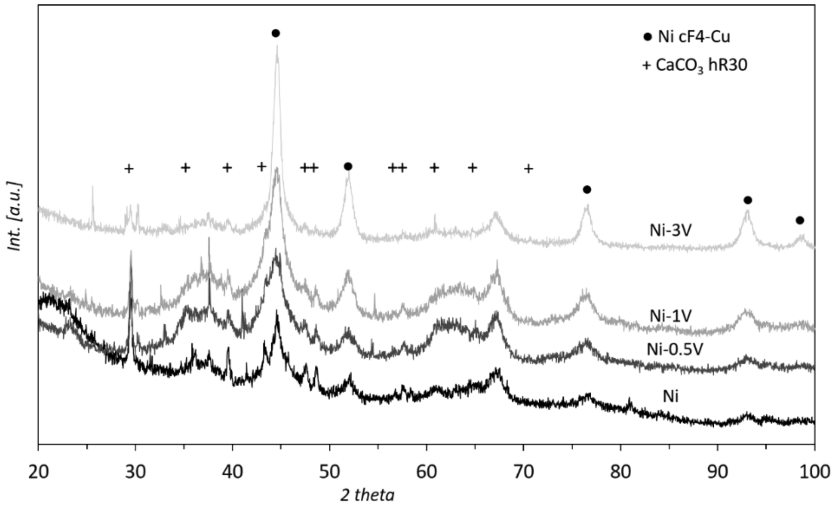

Figure 10. XRD of spent catalysts, after the CO_2 methanation experiment, impured by calcined sand used as a diluent in the catalytic bed.

and 7.4−18.3 × 10^{-3} s^{-1} at 200 °C for MoO_x- and La_2O_3-modified Ni/SiO_2 catalysts (6 wt % Ni).[46]

The results of our study show substantial TOF value differences at the temperature of 523 K. Taking into account the decrease of specific Ni surface area and the TOF value increase with increasing vanadium loading, it appears that Ni/Al_2O_3 doping with V_2O_5 creates Ni−V surface species of higher activity toward CO_2 conversion. Despite the lower number of Ni atoms exposed on the Ni−*x*V surface compared to the vanadia-free catalyst, vanadia doping of the Ni-based catalysts enhances the Ni-specific activity resulting in higher CO_2 conversion per single active site exposed. This conclusion is valid for a moderate vanadia content (up to 1 wt %) and in very good agreement with the H_2-TPR results. The opposite effect was observed for the higher V_2O_5 loading. Therefore, it is justified to conclude that both the Ni surface area and the modification of the surface Ni species with vanadia are crucial for the Ni-based catalyst's final catalytic effect. The V_2O_5 over addition results in a decrease of the catalytic activity, mainly due to the formation of worse dispersed and less reducible nickel active sites with significantly lower activity per active site.

The obtained data show that the catalysts with an intermediate V content, i.e., Ni-0.5V and Ni-1V, have very high activity in the methanation reaction without CO formation. The best temperature to achieve maximum methane yield is 623 K. For laboratory-scale stability testing, and no significant activity/selectivity changes were recorded for more than 30 h at 623 K and 1 atm.[27] In Table 4, we compare our data with the data obtained for the same conditions with other previously tested catalytic materials. One can conclude that the Ni-0.5 V and the Ni-1 V catalysts are significantly more active than those previously reported.

Characterization of Spent Catalysts. After the catalytic experiments in CO_2 hydrogenation, the catalysts were characterized by XRD and field emission scanning electron microscopy (FE-SEM). In Figure 10, the X-ray diffraction patterns of the spent catalysts are reported. As expected, for all catalysts, the main features are those assignable to metallic Ni (JCPDS 71-4655), with the characteristic features of the cF4-Cu prototype at 44.72°, 52.19°, 76.49°, 93.14°, and 98.81° in 2θ. Vanadium can largely enter a cubic solid solution alloy with nickel.[47] In our case, the alloy formation cannot be excluded because no other vanadium compounds are observed in the XRD patterns of the spent catalyst. The peak observed in all cases at 2θ = 67° is assignable to the presence of γ-alumina. The sharp features observed in all diffraction patterns are instead assignable to residuals of the material used as a diluent in the catalytic experiments (not shown).

Figure S2 shows the SEM images of the spent catalysts. The SEM images of the V-free spent catalyst (Figure S2a and b) reveal that Ni forms crystals from 15 to 300 nm in diameter, which are not homogeneously distributed on the catalyst surface. Moreover, the smaller nanoparticles are agglomerated in some parts of the alumina supports, as shown in Figure S2b. The back-scattered electron (BSE) SEM images of Ni−*x*V, shown in Figure S2c and d, exhibit that the sample is not entirely homogeneous considering both the composition and morphology. This is in good agreement with the adopted synthetic procedure and the harsh procedure applied for the reduction step. Metals, i.e., Ni and the (Ni, V) solid solution possibly

https://doi.org/10.1021/acs.iecr.0c05556
Ind. Eng. Chem. Res. 2021, 60, 6554−6564

formed, are found with particles in the range of 15−300 nm. Vanadium content ranges in between 0.1 and 2.7 wt %, while Ni is found with 20−50 wt % loading.

DISCUSSION

This work points out that many of the obtained catalysts show very good activity and selectivity in CO_2 methanation. As said, for the best conditions (623 K), methane is found as the only product, with a very high CO_2 conversion (97%). The preparation of the catalyst was chosen to have extra-durable materials useful for industrial application.[26] Indeed, the data indicate that the materials obtained, both before and after the reaction, are quite heterogeneous with a very limited dispersion of nickel both in the form of NiO in the unreduced fresh catalyst and Ni metal in the spent catalyst. It seems likely that the presence of (formally) CaO tends to limit the dispersion of Ni^{2+}, which is complete when alumina only is present as the support. Presumably, the used composition allows NiO nanoparticle production of intermediate sizes, which results, by reduction, into metallic nickel particles. As previously reported, small cubic nickel nanocrystals are very selective in the methanation, while larger nickel particles are more active on the rWGS reaction.[18] In fact, our V-free Ni catalyst, which contains Ca oxide as the Johnson Matthey JM57-4Q catalyst, exhibits lower activity than the Ni−Al_2O_3 catalysts in the methanation (Table 4). However, the presence of vanadium clearly modifies the situation. In particular, V significantly modifies the NiO particles' reducibility, changing the reduction profiles of nickel species, i.e., not completely associated with spinel, NiO bulk, and small NiO crystallites as shown by TPR. Thus, a V−Ni interaction is quite evident. Even if this is not proven here, it is possible (and not excluded by our data) that the reducible element vanadium enters nickel particles forming a cubic solid solution known to be stable and improves catalytic activity.

CONCLUSIONS

The main conclusions arising from this work are briefly summarized as follows:

(1) The proposed methodology can be applied successfully to the preparation of active catalytic powders and extrudates of potential use in industrial reactors.

(2) The physicochemical characterization data provide evidence of a significantly different structure of the V-free catalyst from the V_2O_5-containing ones. In particular, vanadia modifies the reducibility of NiO as evidenced by TPR experiments.

(3) All catalysts are active for the CO_2 hydrogenation in the investigated temperature range of 523−773 K and atmospheric pressure. However, Ni−V catalysts with the intermediate vanadium loading of 0.5 and 1 wt % are markedly more active than those without vanadium and higher vanadium content. Over these catalysts, 97% methane yield with no CO production is obtained at 623 K.

(4) The catalysts with such an optimal vanadia content are also markedly more active than the previously tested catalysts based on Ni/Al_2O_3 containing SiO_2 and/or La_2O_3, and also than a Ni/Ca aluminate catalyst, in the selective methanation of carbon dioxide.

(5) According to the presented data, the higher catalytic activity of V-containing samples can be related to the Ni surface area. Despite the lower number of Ni atoms exposed on the surface in Ni−xV/Al_2O_3 systems compared to the vanadia-free one, the catalysts doping with vanadia enhance Ni-specific activity resulting in higher CO_2 conversion per single active site exposed.

ASSOCIATED CONTENT

Supporting Information

The Supporting Information is available free of charge at https://pubs.acs.org/doi/10.1021/acs.iecr.0c05556.

XPS data and SEM data (PDF)

AUTHOR INFORMATION

Corresponding Authors

Guido Busca − *Dipartimento di Ingegneria Civile, Chimica e Ambientale (DICCA), Università degli Studi di Genova, 16145 Genova, Italy; Consorzio Interuniversitario Nazionale per la Scienza e Tecnologia dei Materiali, UDR Genova, 16146 Genova, Italy;* orcid.org/0000-0002-5682-2682; Email: Guido.Busca@unige.it

Izabela S. Pieta − *Institute of Physical Chemistry, Polish Academy of Sciences, 01-224 Warsaw, Poland;* orcid.org/0000-0002-3394-7116; Email: ipieta@ichf.edu.pl

Authors

Gabriella Garbarino − *Dipartimento di Ingegneria Civile, Chimica e Ambientale (DICCA), Università degli Studi di Genova, 16145 Genova, Italy; Consorzio Interuniversitario Nazionale per la Scienza e Tecnologia dei Materiali, UDR Genova, 16146 Genova, Italy*

Paweł Kowalik − *Lukasiewicz Research Network - New Chemical Syntheses Institute, 24-110 Pulawy, Poland*

Paola Riani − *Dipartimento di Chimica e Chimica Industriale (DCCI), Università degli Studi di Genova, 16146 Genova, Italy; Consorzio Interuniversitario Nazionale per la Scienza e Tecnologia dei Materiali, UDR Genova, 16146 Genova, Italy;* orcid.org/0000-0002-8629-1819

Katarzyna Antoniak-Jurak − *Lukasiewicz Research Network - New Chemical Syntheses Institute, 24-110 Pulawy, Poland*

Piotr Pieta − *Institute of Physical Chemistry, Polish Academy of Sciences, 01-224 Warsaw, Poland;* orcid.org/0000-0003-0341-2310

Agnieszka Lewalska-Graczyk − *Institute of Physical Chemistry, Polish Academy of Sciences, 01-224 Warsaw, Poland*

Wojciech Lisowski − *Institute of Physical Chemistry, Polish Academy of Sciences, 01-224 Warsaw, Poland*

Robert Nowakowski − *Institute of Physical Chemistry, Polish Academy of Sciences, 01-224 Warsaw, Poland;* orcid.org/0000-0002-8103-3044

Complete contact information is available at: https://pubs.acs.org/10.1021/acs.iecr.0c05556

Author Contributions

I.S.P. designed the catalyst formulation and managed the project. P.K. and K.A.-J. performed the synthesis of catalysts samples and kinetic calculations. G.G., P.R., and G.B. conducted the activity study at the lab-scale level, IR study and postreaction XRD, and SEM characterization. I.S.P., P.P., R.N. conducted lab- and pilot-scale testing, spent catalyst characterization, and patent. I.S.P., P.K., K.A.-J., W.L., and A.L.-G. conducted catalyst characterization and activity analysis. I.S.P., P.P., W.L., P.K., K.A.-J., and G.G. conducted data processing. I.S.P., R.N., P.K., K.A.-J., G.B., G.G., and P.P. analyzed the data. I.S.P. drafted the

https://doi.org/10.1021/acs.iecr.0c05556
Ind. Eng. Chem. Res. 2021, 60, 6554−6564

main text of the manuscript. I.S.P., P.P., P.K. G.G., and G.B. wrote the manuscript. All authors have given their final approval for the manuscript.

Notes

The authors declare no competing financial interest.

■ ACKNOWLEDGMENTS

This research was supported by receiving funding from the Foundation for Polish Science Reintegration/2016-1/5 Project "Waste to fuel—Catalyst and process development for waste biomass valorization", cofinanced by the European Regional Development Fund under the Intelligent Development Operational Program 2014−2020 (POIR), Axis IV: Increasing the scientific and research potential, Measure 4.4: Increasing the human potential in the R&D sector, awarded to I.S.P., with connected subcontracting agreement 1414/2018 given to G.G. for the Task "CO_2 valorization over V-modified Ni catalyst supported on various supports". I.S.P. gratefully acknowledges support from the French Government for collaboration with Sorbonne University Project "Catalytic conversion of CO_2 to hydrocarbons: The Ni−V catalyst selectivity and durability in in plasma assisted hydrogenation of CO_2 to methane". GG, PR and GB acknowledge University of Genova, Fondo Incentivazione Europea.

■ REFERENCES

(1) Senderens, J.-B.; Sabatier, P. Nouvelles synthèses du methane. *C. R. Acad. Sci.* **1902**, *82*, 514−516.
(2) Sabatier, P.; Senderens, J.-B. Hydrogénation directe des oxydes du carbone en présence de divers métaux divisés. *C. R. Acad. Sci.* **1903**, *134*, 689−691.
(3) Brightling, J. Ammonia and the fertiliser industry: the development of ammonia at Billingham. *Johnson Matthey Technol. Rev.* **2018**, *62*, 32−47.
(4) Clariant. *Catalysts and Adsorbents for Syngas*. https://www.clariant.com/en/Business-Units/Catalysts/Syngas-Catalysts (accessed April 2021).
(5) Johnson Matthey, *Catalysts for Olefin Processes*. https://matthey.com/-/media/files/markets/jm-catalysts-for-olefin-processes.pdf (accessed April 2021).
(6) INS Pulawy. *Commercial Methanation Catalysts*. http://www.ins.pulawy.pl/index.php/en/products/catalysts-and-sorbents/methanation (accessed on 06. 03. 2021).
(7) Rönsch, S.; Schneider, J.; Matthischke, S.; Schlüter, M.; Götz, M.; Lefebvre, J.; Prabhakaran, P.; Bajohr, S. Review on methanation - From fundamentals to current projects. *Fuel* **2016**, *166*, 276−296.
(8) Höhlein, B.; Menzer, R.; Range, J. High temperature methanation in the long-distance nuclear energy transport system. *Appl. Catal.* **1981**, *1*, 125−139.
(9) National Energy Technology Laboratory. *Great Plains Synfuels Plant*. https://netl.doe.gov/research/Coal/energy-systems/gasification/gasifipedia/great-plains#:-:text=The%20Great%20Plains%20Synfuels%20Plant,facility%20in%20the%20United%20States (accessed Feb 15, 2021).
(10) Johnson Matthey. *DAVY*. https://matthey.com/en/products-and-services/chemical-processes/licensed-processes/substitute-natural-gas-process (accessed April 2021).
(11) Topsoe. *TREMP*. https://www.topsoe.com/processes/sng (accessed April 2021).
(12) Ren, J.; Liu, Yi-L.; Zhao, X.-Y.; Cao, J.-P. Methanation of syngas from biomass gasification: an overview. *Int. J. Hydrogen Energy* **2020**, *45*, 4223−4243.
(13) Ashok, J.; Pati, S.; Hongmanorom, P.; Tianxi, Z.; Junmei, C.; Kawi, S. A review of recent catalyst advances in CO2 methanation processes. *Catal. Today* **2020**, *356*, 471−489.
(14) Braga, A. H.; Vidinha, P.; Rossi, L. M. Hydrogenation of carbon dioxide: From waste to value. *Current Opin. Green Sust. Chem.* **2020**, *26*, 100386.
(15) Chwoła, T.; Spietz, T.; Więcław-Solny, L.; Tatarczuk, A.; Krótki, A.; Dobras, S.; Wilk, A.; Tchórz, J.; Stec, M.; Zdeb, J. Pilot plant initial results for the methanation process using CO2 from amine scrubbing at the Łaziska power plant in Poland. *Fuel* **2020**, *263*, 116804.
(16) NASA. *The Sabatier System: Producing Water on the Space Station*. https://www.nasa.gov/mission_pages/station/research/news/sabatier.html (accessed Feb 15, 2021).
(17) Dannesboe, C.; Hansen, J. B.; Johannsen, Ib Catalytic methanation of CO2 in biogas: experimental results from a reactor at full scale. *React. Chem. Eng.* **2020**, *5*, 183−189.
(18) Garbarino, G.; Riani, P.; Magistri, L.; Busca, G. A study of the methanation of carbon dioxide on Ni/Al2O3 catalysts at atmospheric pressure. *Int. J. Hydrogen Energy* **2014**, *39*, 11557−11565.
(19) Garbarino, G.; Bellotti, D.; Riani, P.; Magistri, L.; Busca, G. Methanation of carbon dioxide on Ru/Al2O3 and Ni/Al2O3 catalysts at atmospheric pressure: catalysts activation, behaviour and stability. *Int. J. Hydrogen Energy* **2015**, *40*, 9171−9182.
(20) Garbarino, G.; Wang, C.; Cavattoni, T.; Finocchio, E.; Riani, P.; Flytzani-Stephanopoulos, M.; Busca, G. A study of Ni/La-Al2O3 catalysts: a competitive system for CO2Methanation. *Appl. Catal., B* **2019**, *248*, 286−297.
(21) Riani, P.; Valsamakis, I.; Cavattoni, T.; Sanchez Escribano, V.; Busca, G.; Garbarino, G. Ni/SiO2-Al2O3 catalysts for CO2 methanation: effect of La2O3 addition. *Appl. Catal., B* **2021**, *284*, 119697.
(22) Carlsson, M. Carbon Formation in Steam Reforming and Effect of Potassium Promotion. *Johnson Matthey Technol. Rev.* **2015**, *59*, 313−318.
(23) Garbarino, G.; Pugliese, F.; Cavattoni, T.; Busca, G.; Costamagna, P. A study on CO2 methanation and Steam Methane Reforming over commercial Ni/calcium aluminate catalysts. *Energies* **2020**, *13*, 2792.
(24) Kowalik, P.; Antoniak-Jurak, K.; Błesznowski, M.; Herrera, M. C.; Larrubia, M. A.; Alemany, L. J.; Pieta, I. S. Biofuel steam reforming catalyst for fuel cell application. *Catal. Today* **2015**, *254*, 129−134.
(25) Gonzalez-Gil, R.; Herrera, C.; Larrubia, M. A.; Kowalik, P.; Pieta, I. S.; Alemany, L. J. Hydrogen production by steam reforming of DME over Ni-based catalysts modified with vanadium. *Int. J. Hydrogen Energy* **2016**, *41*, 19781−19788.
(26) Pieta, I. S. The method and installation for continuous multi-parameter analysis of gaseous fuel conversion including reforming and measurement of post-reaction gas pollutants nitrogen, carbon and sulfur oxides and chlorine. Polish Patent P-412277, 2015.
(27) Pieta, I. S.; Pieta, P.; Nowakowski, R. Nickel-vanadium catalyst for the valorization of carbon dioxide, a method of obtaining a nickel-vanadium catalyst and the use of a nickel-vanadium catalyst in the processes of carbon dioxide hydrogenation and reforming. Polish Patent P-434122, 2020.
(28) García-Diéguez, M.; Pieta, I. S.; Herrera, M. C.; Larrubia, M. A.; Alemany, L. J. Nanostructured Pt- and Ni-based catalysts for CO2-reforming of methane. *J. Catal.* **2010**, *270*, 136−145.
(29) Rodriguez-Blanco, J. D.; Shaw, S.; Benning, L. G. The kinetics and mechanisms of amorphous calcium carbonate (ACC) crystallization to calcite, viavaterite. *Nanoscale* **2011**, *3*, 265−271.
(30) Busca, G. The surface of transition aluminas. A critical Review. *Catal. Today* **2014**, *226*, 2−13.
(31) Garbarino, G.; Campodonico, S.; Perez, A. R.; Carnasciali, M. M.; Riani, P.; Finocchio, E.; Busca, G. Spectroscopic characterization of Ni/Al2O3 catalytic materials for the steam reforming of renewables. *Appl. Catal., A* **2013**, *452*, 163−173.
(32) Kloprogge, J. T.; Ruan, H. D.; Frost, R. L. Thermal decomposition of bauxite minerals: infrared emission spectroscopy of gibbsite, boehmite and diaspore. *J. Mater. Sci.* **2002**, *37*, 1121−1129.
(33) Larrubia, M. A.; Busca, G. An ultraviolet-visible-infrared study of the electronic structure of oxide supported vanadia-tungsta and vanadia-molybdena. *Mater. Chem. Phys.* **2001**, *72*, 337−346.

https://doi.org/10.1021/acs.iecr.0c05556
Ind. Eng. Chem. Res. 2021, 60, 6554−6564

(34) Garbarino, G.; Wang, C.; Cavattoni, T.; Finocchio, E.; Riani, P.; Flytzani-Stephanopoulos, M.; Busca, G. A study of Ni/La-Al2O3 catalysts: a competitive system for CO2Methanation. *Appl. Catal., B* **2019**, *248*, 286−297.
(35) Garbarino, G.; Riani, P.; Infantes-Molina, A.; Rodríguez-Castellón, E.; Busca, G. On the detectability limits of nickel species on NiO//-Al2O3 catalytic materials. *Appl. Catal., A* **2016**, *525*, 180−189.
(36) Lemonidou, A. A.; Goula, M. A.; Vasalos, I. A. Carbon dioxide reforming of methane over 5 wt.% nickel calcium aluminate catalysts ± effect of preparation method. *Catal. Today* **1998**, *46*, 175−183.
(37) Scheffer, B.; Molhoek, P.; Moulijn, J. A. Temperature-programmed reduction of NiO single bond WO3/Al2O3 Hydro-desulphurization catalysts. *Appl. Catal.* **1989**, *46*, 11−30.
(38) Rogers, J. L.; Mangarella, M. C.; D'Amico, A. D.; Gallagher, J. R.; Dutzer, M. R.; Stavitski, E.; Miller, J. T.; Sievers, C. Differences in the Nature of Active Sites for Methane Dry Reforming and Methane Steam Reforming over Nickel Aluminate Catalysts. *ACS Catal.* **2016**, *6*, 5873−5886.
(39) Sahli, N.; Petit, C.; Roger, A. C.; Kiennemann, A.; Libs, S.; Bettahar, M. M. Ni catalysts from NiAl2O4 spinel for CO2 reforming of methane. *Catal. Today* **2006**, *113*, 187−193.
(40) Liu, Q.; Gu, F.; Lu, X.; Liu, Y.; Li, H.; Zhong, Z.; Xu, G.; Su, F. Enhanced catalytic performances of Ni/Al2O3 catalyst via addition of V2O3 for CO methanation. *Appl. Catal., A* **2014**, *488*, 37−47.
(41) Ruitenbeek, M.; van Dillen, A. J.; de Groot, F. M. F.; Wachs, I. E.; Geus, J. W.; Koningsberger, D. C. The structure of vanadium oxide species on-alumina;anin situX-ray absorption study during catalytic oxidation. *Top. Catal.* **2000**, *10*, 241−254.
(42) Vogt, C.; Monai, M.; Sterk, E. B.; Palle, J.; Melcherts, A. E. M.; Zijlstra, B.; Groeneveld, E.; Berben, P. H.; Boereboom, J. M.; Hensen, E. J. M.; Meirer, F.; Filot, I. A. W.; Weckhuysen, B. M. Understanding carbon dioxide activation and carbon−carbon coupling over nickel. *Nat. Commun.* **2019**, *10*, 5330.
(43) Liu, Q.; Wang, S.; Zhao, G.; Yang, H.; Yuan, M.; An, X.; Zhou, H.; Qiao, Y.; Tian, Y. CO2 methanation over ordered mesoporous NiRu-doped CaO-Al2O3 nanocomposites with enhanced catalytic performance. *Int. J. Hydrogen Energy* **2018**, *43*, 239−250.
(44) Quindimil, A.; De-La-Torre, U.; Pereda-Ayo, B.; Davó-Quiñonero, A.; Bailón-García, E.; Lozano-Castelló, D.; González-Marcos, J. A.; Bueno-López, A.; González-Velasco, J. R. Effect of metal loading on the CO2 methanation: A comparison between alumina supported Ni and Ru catalysts. *Catal. Today* **2020**, *356*, 419−432.
(45) Qin, Z.; Zhou, Y.; Jiang, Y.; Liu, Z.; Ji, H. Recent Advances in Heterogeneous Catalytic Hydrogenation of CO_2 to Methane. In *New Advances in Hydrogenation Processes - Fundamentals and Applications*; Ravanchi, M. T., Ed.; IntechOpen, 2017. DOI: 10.5772/65407. https://www.intechopen.com/books/new-advances-in-hydrogenation-processes-fundamentals-and-applications/recent-advances-in-heterogeneous-catalytic-hydrogenation-of-co2-to-methane (accessed on Feb 02, 2021).
(46) Li, S.; Guo, S.; Gong, D.; Kang, N.; Fang, K.-G.; Liu, Y. Nano composite composed of MoOx- La2O3Ni on SiO2 for storing hydrogen into CH4 via CO2 methanation. *Int. J. Hydrogen Energy* **2019**, *44*, 1597−1609.
(47) Smith, J. F.; Carlson, O. N.; Nash, P. G. The Ni-V (Nickel-vanadium) system. *Bull. Alloy Phase Diagrams* **1982**, *3*, 342−348.

https://doi.org/10.1021/acs.iecr.0c05556
Ind. Eng. Chem. Res. 2021, 60, 6554−6564